coatings

MDPI

Article

Effect of Cutting Insert Shape and Roughness on Built-Up Edge Formation When Cutting Steel AISI 316L

Saulius Baskutis [1], Egidijus Dragašius [1], Audrius Žunda [2,3,*], Albinas Andriušis [2], Raimondas Kreivaitis [2], Simona Tučkutė [4] and Oleksandr Kapustynskyi [3]

[1] Faculty of Mechanical Engineering and Design, Kaunas University of Technology, 51424 Kaunas, Lithuania; saulius.baskutis@ktu.lt (S.B.); egidijus.dragasius@ktu.lt (E.D.)
[2] Faculty of Engineering, Agriculture Academy of Vytautas Magnus University, 53361 Akademija, Lithuania; albinas.andriusis@vdu.lt (A.A.); raimondas.kreivaitis@vdu.lt (R.K.)
[3] Faculty of Mechanics, Vilnius Gediminas Technical University—VilniusTech, 10223 Vilnius, Lithuania; o.kapustynskyi@vilniustech.lt
[4] Center for Hydrogen Energy Technologies, Lithuanian Energy Institute, 44409 Kaunas, Lithuania; simona.tuckute@lei.lt
* Correspondence: audrius.zunda@vdu.lt; Tel.: +370-675-27255

Abstract

In general, the properties of alloy steels and special steels provide significant advantages to the end product. However, these properties often complicate the machining process, particularly in terms of machinability. The formation of a built-up edge (BUE) is a widely recognized phenomenon in the machining of austenitic stainless steels. It is closely associated with changes in cutting performance, tool wear, and surface integrity. Complex adhesive and plastic deformation processes drive BUE development under severe contact conditions at the tool–chip interface. Consequently, the geometrical characteristics and surface roughness of cutting inserts are expected to significantly influence the initiation and growth of adhered material layers on the cutting edge. The insert shape dictates the cutting forces and chip flow. In contrast, insert roughness (and micro-geometry) strongly influences friction and material sticking at the tool–chip interface. This article analyzes the processes in the material-tool contact system and their relationship to geometry, rake-face surface parameters, and BUE development when turning AISI 316L steel under dry and minimal lubrication conditions. The results indicate that BUE development is associated with the combined effects of chip-breaker geometry, rake-face roughness parameters (R_q, R_{sk}, and R_{ku}), and cutting conditions. Cooling, including the use of an ionic liquid–water suspension, reduces the insert's susceptibility to adhesion.

Keywords: rake surface roughness; build-up edge; cutting speed; insert shape

Check for updates

Academic Editor: Stefano Rossi

Received: 26 July 2026
Revised: 11 September 2026
Accepted: 15 September 2026
Published: 20 September 2026

Copyright: © 2026 by the authors. Licensee MDPI, Basel, Switzerland. This article is an open access article distributed under the terms and conditions of the Creative Commons Attribution (CC BY) license.

1. Introduction

According to various sources, the global alloy steel market was valued at approximately USD 91–96 billion in 2026 and is expected to reach more than USD 170 billion in 2035 [1,2]. Most of these steels are austenitic and are used in automation, transportation, mechanical engineering, and heavy industry. Therefore, the machinability of these steels will remain relevant for several decades. The sensitivity of austenitic steel machinability is also evident in the work of scientists who have optimized cutting parameters and increased tool life through experimental and computational studies over the past ten years.

The review on the machining of austenitic stainless steels [3–5] shows the factors influencing the machinability of 300-grade steels that have been determined by experimental

studies, such as the surface quality and geometry of the cutting insert, the size of the structural grains in the steel microstructure, the chemical composition, cutting parameters, and coolants. Such studies help improve cutting tools, identify optimum cutting parameters, and explore possibilities for sustainable machining.

One criterion for assessing a material's machinability is the roughness of the resulting surface. It is well established that the roughness of the cylindrical surface during turning, regardless of the type of material, is most influenced by the cutting speed and feed rate. Recent studies identify additional factors that shape the roughness profile for specific alloys. Leksycki et al. [6] show that when machining AISI 316L steel, in addition to the "thread-like" trace traditionally left by the tip of the cutting tool, plastic slip flow often forms across the entire cutting speed (V_c) range of 150–500 m/min. The study also showed that the surface roughness parameter Rz decreases in the range of cutting speeds 280–420 m/min and feed rates (f) 0.1–0.2 mm/rev, while it increases in the range of cutting speeds 190–460 m/min and feed rates 0.2–0.35 mm/rev. Nur et al. [7] investigated AISI 316L steel and found that cutting speed was inversely proportional to tool life, but that surface roughness and cutting force were not significantly affected. The feed rate was found to be directly proportional to cutting force and surface roughness, but inversely proportional to tool life. Other authors assumed that the critical factors for BUE formation in stainless steels are cutting speed, cutting temperature, microcrack formation, feed rate, tool rake angle, and tool rake temperature [8–10].

Rake parameters are also important in BUE formation. Insert shape involves both the macro-geometry (ISO turning insert shape "W" trigon 80° in our case, nose radius, rake angles, chip breaker) and micro-geometry (cutting edge radius, chamfers, roughness). A larger nose radius spreads cutting forces over a wider area, lowering temperatures slightly but increasing contact length. This prolongs the time the chip spends in contact with the rake face, which can increase the likelihood of a BUE forming if cutting speeds are not high enough [11,12]. Positive rake angles reduce cutting forces and shear deformation, promoting cleaner material removal and minimizing BUE formation. In contrast, negative rake angles promote severe plastic deformation and increase friction, significantly worsening BUE accumulation [8,13]. Micro-Geometry: A larger cutting-edge radius (e.g., increasing from 4 μm to 12 μm) increases cutting forces but improves edge strength. Smaller edge radii (sharper tools) are preferred for AISI 316L as they reduce plowing and delay the onset of the BUE, although they make the tool prone to chipping when the BUE breaks off [8,9,14,15]. Insert surface roughness also affects BUE formation. The surface finish, or texture, of the cutting insert directly governs friction and adhesive affinity between the stainless-steel chip and the tool. For smooth rake faces, a highly polished insert reduces the coefficient of friction and prevents the aggressive pressure-welding of the highly ductile AISI 316L chip to the tool surface. This decreases the size and stability of the BUE [8]. However, when high surface roughness anchors the steel chip, it traps heat and facilitates material adhesion. This creates a highly stable BUE that oscillates in size, causing dimensional inaccuracies in the part [8]. A modern trend highlighted in the literature is the use of laser-textured rake faces with micro-holes or grooves that reduce the physical contact area between the chip and the tool. Such textures can trap lubricants or create air pockets that restrict BUE formation and adherence when machining AISI 316L [8,13].

Recent academic literature on machining AISI 316L emphasizes several critical factors. Studies on tool life and coatings note that combining smooth Physical Vapor Deposition (PVD)-coated inserts (such as TiAlSiN or Al_2O_3) with polished or textured rake faces reduces frictional heat, preventing the steel from welding to the insert [8]. Cutting velocity is a prominent factor in BUE formation during finishing or slower-speed operations (e.g., 60 m/min), and scholars frequently recommend increasing cutting speeds above

150 m/min to raise shear-plane temperature and soften the material, thereby inhibiting the BUE [8,11]. The BUE affects surface integrity; when the BUE loosens, it often removes microscopic pieces of the cutting-tool substrate (chipping) and leaves adhered material on the finished AISI 316L surface, destroying the desired surface roughness of the workpiece [8,11].

Tool wear depends strongly on whether cutting is performed with or without cooling and lubrication. Previous studies indicate that at the beginning of cutting, lubrication has little effect on tool wear, but later the situation changes, and cooling and lubrication become significant factors that increase tool longevity [16,17]. Interestingly, lubrication did not significantly affect BUE formation or adhesive wear. Recently, ionic liquids (ILs) have gained popularity as cutting fluids. The authors [18,19] report reduced treated surface roughness, power consumption, cutting temperature, carbon emissions, noise emission, circularity error, and tool wear under ionic fluid conditions. Other studies show that intense tool wear begins in the first few seconds of operation. Wear craters formed on the rake face of the indexable insert after only 12 s. Tool wear, characterized by crater formation on the insert, is driven by a diffuse wear mechanism [20]. Gerth et al. [21] also observed stronger adhesion between the tool and the chip when turning AISI 316L steel. In diffuse or adhesive tool wear, traces of adhesive degradation should also be visible on the chip, namely on the side that slides against the tool surface.

Beyond frequently reported Ra and Rz metrics, additional profile roughness parameters—including R_q, R_{sk}, and R_{ku}—offer further insight into surface texture [22–24]. R_q quantifies the amplitude of profile-height fluctuations, while R_{sk} indicates the asymmetry (skewness) of the profile-height distribution, and R_{ku} reflects its kurtosis. Together, these measures describe aspects of the surface-height distribution that Ra alone does not capture. Although they are commonly used to characterize engineering surfaces, their application to cutting-tool rake faces and any potential links to BUE formation have been explored relatively little.

The modern metalworking industry is dominated by Computer Numerical Control (CNC) machines; however, manually controlled lathes (MCL) are still used to produce individual parts. In the past decade, research has also examined cutting steel with manually controlled machines [25]. One of the main differences and disadvantages of these machines is the gradual adjustment of spindle speed. In contrast to CNC machines, for example, where revolutions increase evenly as the workpiece diameter decreases (V_c must remain constant), this happens gradually with MCL. This means that the cut is performed during a certain working time with decreasing V_c. This affects the cutting process, including chip and BUE formation.

The purpose of this work was to analyze the relationship between cutting insert surface parameters (chip-breaker type, R_q, R_{sk}, and R_{ku}) and built-up edge (BUE) development, as well as the impact of cutting parameters—cutting speed (V_c), feed (f), and cutting depth (ap)—on BUE formation when turning AISI 316L steel with manually controlled machines under dry and minimum quantity lubrication (MQL) conditions using ILs.

2. Materials and Methods

An AISI 316L steel bar (Laxcon Steels, Taluka Sanand, India) with a diameter of 40 mm was used for the turning tests. The work was carried out using a universal manually operated lathe 16K20 (Stankoimport, Moscow, Russia). This is not a disadvantage when working at fixed cutting speeds compared to CNC machines. To measure the cutting forces, we modified a standard lathe tool holder M02L012320M08 (KIZ, Kirzhach, Russia) suitable for WNMG inserts by installing stress gages (see Figure 1) of type SGT-1/350-TY11 (Omega Engineering Inc., Norwalk, CT, USA) in a full-bridge configuration, with natural Poisson

and temperature compensation. Before the test, the modified insert holder was calibrated with a dynamometer DOSM-3-0,2 rated at 2000 N (ZIP, Moscow, Russia).

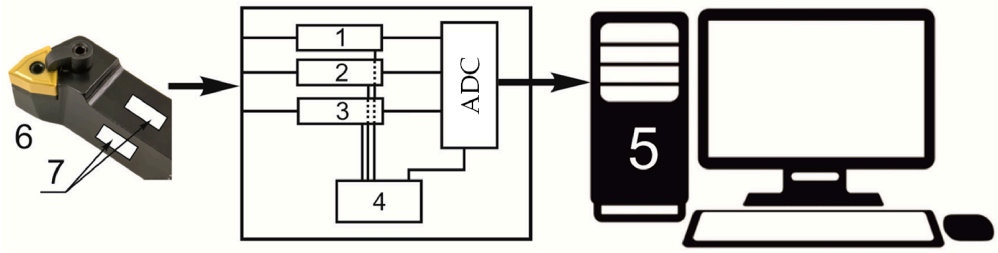


Figure 1. Schematic diagram of cutting force measurement: 1, 2, and 3—Omega TX DIN 1200S amplifiers; 5—PC; 6—turning tool; 7—piezoresistive gauges; ADC—analog-to-digital converter.

The experiment used 3 different WNMG 080408 inserts (GARANT 252070 HB730-1 and GARANT 252070 HB7120-1 (Hoffmann Group, Nuremberg, Germany), Kyocera WNMG080408MS (Kyocera Corporation, Kyoto, Japan). Figure 2 shows the cutting test schematics.

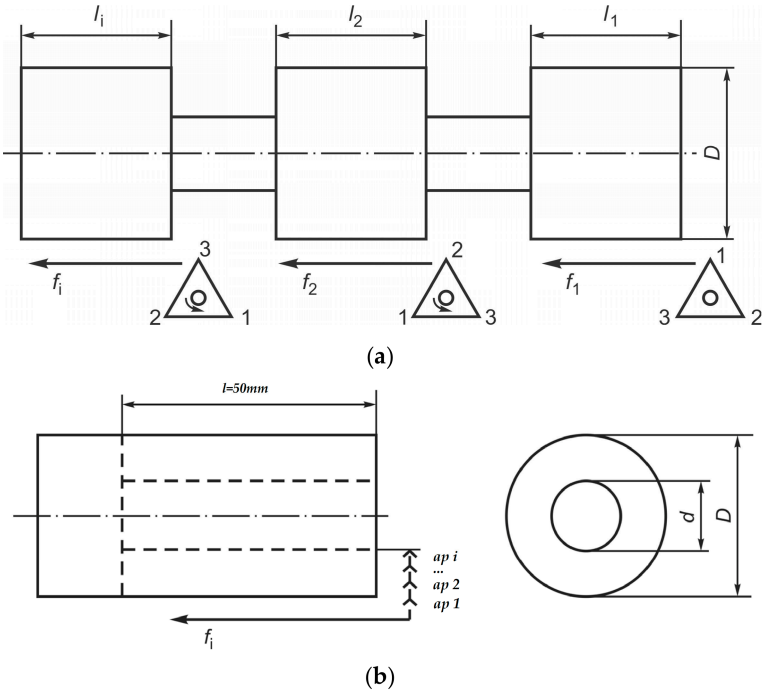


Figure 2. Cutting-test scheme: (**a**) one-cycle (T1) cutting conditions; (**b**) multi-cycle (Ti) cutting conditions; l_1–i—cut-surface length; ap1–i—depth of cut and number of pass; *D*—initial workpiece diameter (*D* = 40 mm); 1, 2, and 3—sequence of insert tip usage. Note: $l_1 = l_2 = li$; l = 50 mm = T1 (one work cycle).

A Leica M205C (Leica Microsystems Ltd., Heerbrugg, Switzerland) automated optical stereo microscope with software Leica Application Suite X (version 5.3.0.29166) and a Nikon Eclipse MD 100 (Nikon Metrology NV, Tokyo, Japan) optical microscope with NIS-Elements D4.10.00 software were used for microscopic analysis of the inserts. A scanning electron microscope (SEM) Hitachi 3400N (Hitachi, Tokyo, Japan) and a Bruker Quad 5040 (Bruker, Berlin, Germany) energy-dispersive spectroscopy (EDS) system were used to inspect worn cutting edges. We evaluated the rake-face geometry and surface topography of the cutting inserts using a non-contact CNC vision measurement system (Mitutoyo Quick Vision Hyper, Mitutoyo QCH; Mitutoyo Corp., Kawasaki-shi, Japan). Measurements were collected with Mitutoyo QVPAK v14.1, and three-dimensional surface reconstruction

and profile analyses were conducted in Mitutoyo MCubeMap Ultimate V9. For each insert, we extracted a single profile from the central area of the measured 3D rake-face topography and used it to assess profile roughness. From this profile, we calculated R_a, R_q, R_{sk}, and R_{ku}. R_a denotes the arithmetic mean deviation of the roughness profile, R_q the root-mean-square deviation, R_{sk} the skewness of the profile height distribution, and R_{ku} the kurtosis. We used a Mahr Mar-Surf GD25 (Mahr GmbH, Göttingen, Germany) profilometer with MarSurf XR20 QeRun Application software (vesrion V2.02-25) to analyze the roughness of the treated surfaces.

Table 1 presents the experimental cutting modes. Cutting parameters were selected based on the manufacturer's recommendations (on the insert packaging) and the settings of the manually operated lathe to evaluate their influence on built-up edge formation.

Table 1. Experimental cutting modes.

No.	V_c, m/min	f, mm/rev	ap, mm	* T_1 (T_{15})
1.1.1	157	0.20	0.5	1 (15)
1.1.2		0.20	1.0	1 (15)
1.2.1		0.35	0.5	1 (15)
1.2.2		0.35	1.0	1 (15)
1.3.1		0.50	0.5	1 (15)
1.3.2		0.50	1.0	1 (15)
2.1.1	126	0.20	0.5	1 (15)
2.1.2		0.20	1.0	1 (15)
2.2.1		0.35	0.5	1 (15)
2.2.2		0.35	1.0	1 (15)
2.3.1		0.50	0.5	1 (15)
2.3.2		0.50	1.0	1 (15)

* T_1—short work (cutting) cycle: T_1 = 1 l cut; T_{15}—long work cycle: T_{15} = 15 l cut.

Under T_1 conditions, the outer cylindrical surface was machined in one pass with selected parameters. Under T_{15} conditions, the outer cylindrical surface was machined in several passes (i) at the selected depth of cut ap. The machine spindle speed did not change as the machining diameter varied.

Cutting was performed under dry conditions and with cooling. For cooling, deionized water (DW) and a suspension of deionized water with Bis(2-hydroxyethyl) ammonium erucate (DEE) ionic liquid (IL) at 50% were used. We sprayed the cooling liquid using Aerograf AB-183K (Wenzhou Hanfong Machinery Co., Ltd., Wenzhou, China). The coolant flow rate was 1 g/min. Before cutting, the workpiece and cutting insert surfaces were cleaned with acetone.

3. Results

Figure 3 and Table 2 present the rake-face parameters of the standard WNMG inserts used for the cutting tests. The insert HB7120-1 was a CVD-coated carbide composed of TiCN and Al_2O_3 layers. Insert 432MS had a TiCN + Al_2O_3 + TiN layer. Insert HB730-1 had a TiN coating. Table 2 presents the shapes and roughness parameters of the insert rake faces. Data were obtained using a Leica M205C and a Mitutoyo QVH.

Beyond variations in coating and rake-face texture, the inserts also showed markedly different chip-breaker geometries. From the topography data, the estimated distance from the cutting edge to the closest chip-breaking element was about 1350 µm for HB7120-1, about 2600 µm for 432MS and about 700 µm for HB730-1. Accordingly, when comparing the three inserts, it is important to account for both the rake-face surface texture and its macro-scale geometry.

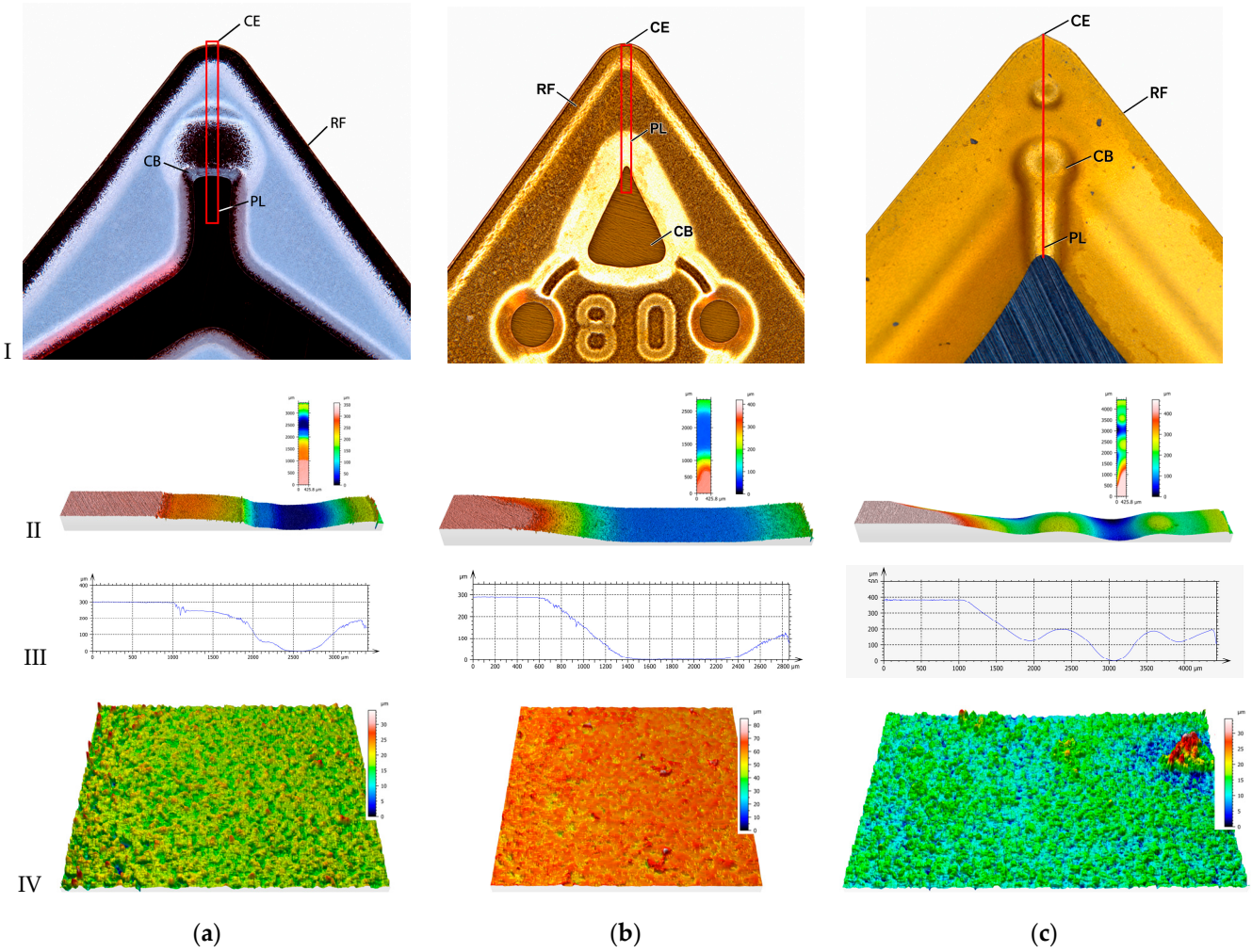


Figure 3. The views of the new WNMG inserts' rake faces: (**a**) HB7120-1; (**b**) 432MS; and (**c**) HB730-1; I—optical image of the insert showing the cutting edge (CE), rake face (RF), chip breaker (CB), and profile line (PL); II—three-dimensional view along the selected profile line; III—extracted surface profile; IV—three-dimensional surface-topography map of the rake face.

Table 2. Geometrical and profile roughness characteristics of the rake face of cutting inserts.

Parameter	HB7120-1	432MS	HB730-1
R_a, µm	0.995	1.242	0.938
R_q, µm	1.257	1.564	1.163
R_{sk}	0.047	0.140	0.162
R_{ku}	2.806	3.644	2.687
Cutting edge–chip breaker distance, µm	~1350	~2600	~700

The values presented in Table 2 were obtained from a single profile measured for each insert; therefore, they characterize the selected rake-face profile.

These results show that the inserts have very different rake-face shapes and chip-breaker geometries (Figure 3). R_q describes the magnitude of the profile-height variations, whereas R_{sk} and R_{ku} characterize the skewness and kurtosis of the profile-height distribution, respectively.

Figure 4 shows views of the face of the inserts after one cycle (T_1) of dry cutting conditions at different cut speeds. It can be observed that, in all cases, the contact zone CZ (Figure 4) between the chip and the tool is clearly visible, with a distinct mark of the chip

edge line (CEL) in the direction of chip flow where the chip separates from the workpiece on the rake face, as well as spots where the chip contacts the rake face further from the edge, forming a BUE, surface build layer (SBU), and a build-up on the chip breaker (CBBU) after just one work cycle. The HB7120-1 insert is not as sensitive to SBU and CBBU as other inserts; however, at lower cutting speeds, a built-up edge forms at the CEL—just as it does on the rake face of other inserts. Furthermore, CBBU growth occurs opposite the chip flow direction on the HB730-1 insert (Figure 4, V_c = 126 m/min). This trend was observed across various cutting parameters as the number of cycles increased for the HB730-1 insert.

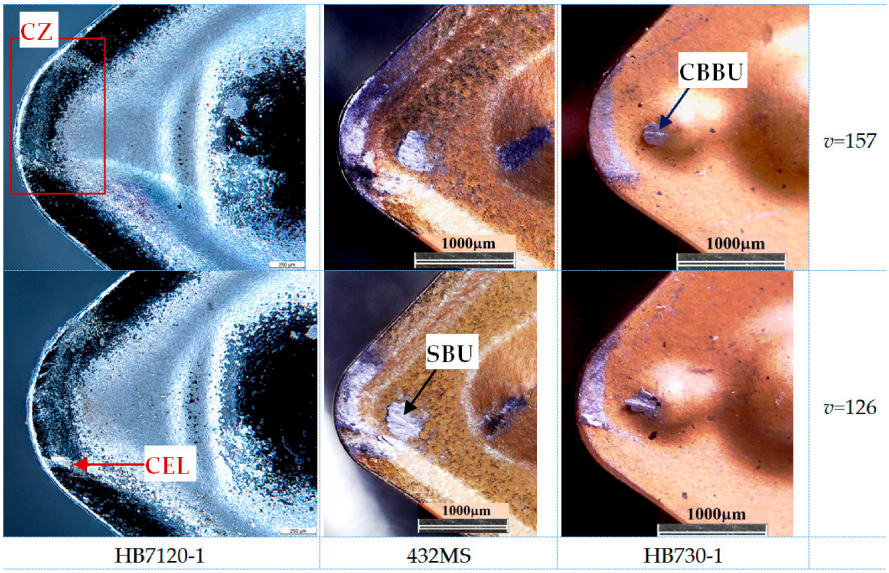


Figure 4. The view of the worn WNMG insert's rake face after the T_1 test: f = 0.5 mm/rev; ap = 1 mm; dry conditions; V_c = 126 m/min.

To determine the actual damage to the rake face, the inserts were etched in a 40% aqueous $FeCl_3$ solution to dissolve the built-up edge (BUE). Figure 5 presents optical and SEM images of the etched inserts that operated at different cutting speeds. The images were obtained using a Nikon Eclipse MD 100 optical microscope and a Hitachi 3400N SEM.

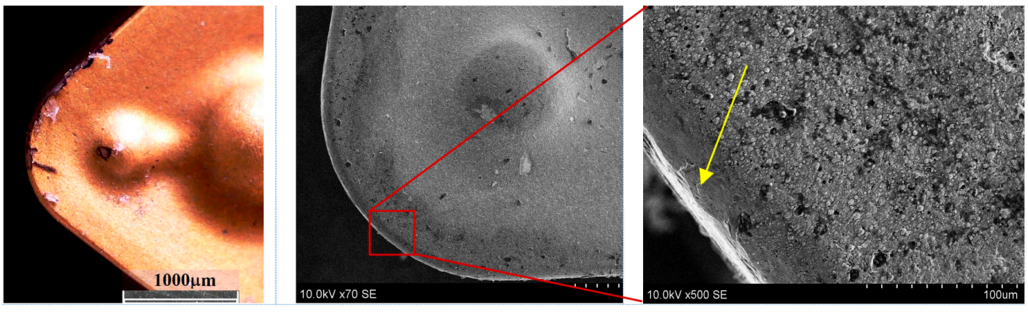


Figure 5. Optical and SEM views of the worn HB730-1 WNMG insert after etching in iron chloride ($FeCl_3$) following the T_1 test: f = 0.5 mm/rev; ap = 1 mm; dry conditions; (**a**) optical view of the insert tip at V_c = 126 m/min; (**b**) and (**c**) SEM views of the insert tip marked section at V_c = 157 m/min.

At the lower cutting speed of 126 m/min, the insert damage is visible in the optical microscope image: clear coating damage on the rake edge and a small spot of worn coating on the chip breaker (Figure 5a). Under *T*1 and 157 m/min conditions, the damage is more visible in the SEM image (Figure 5b,c). The defects are not as pronounced. The most

distinct defects are a spot where the CBBU was located (Figure 5b) and slight chipping of the cutting edge (Figure 5c; yellow arrow).

The results of the multi-cycle cutting test T15 on AISI 316L steel, conducted with and without cooling, are presented below. Figure 6 clearly shows the differences in rake-face conditions across the various machining conditions after the tests. Because these are pilot studies, we present a more detailed analysis only for a cutting speed of 157 m/min. At lower speeds, the damage is more severe, necessitating further research involving more intensive cooling.

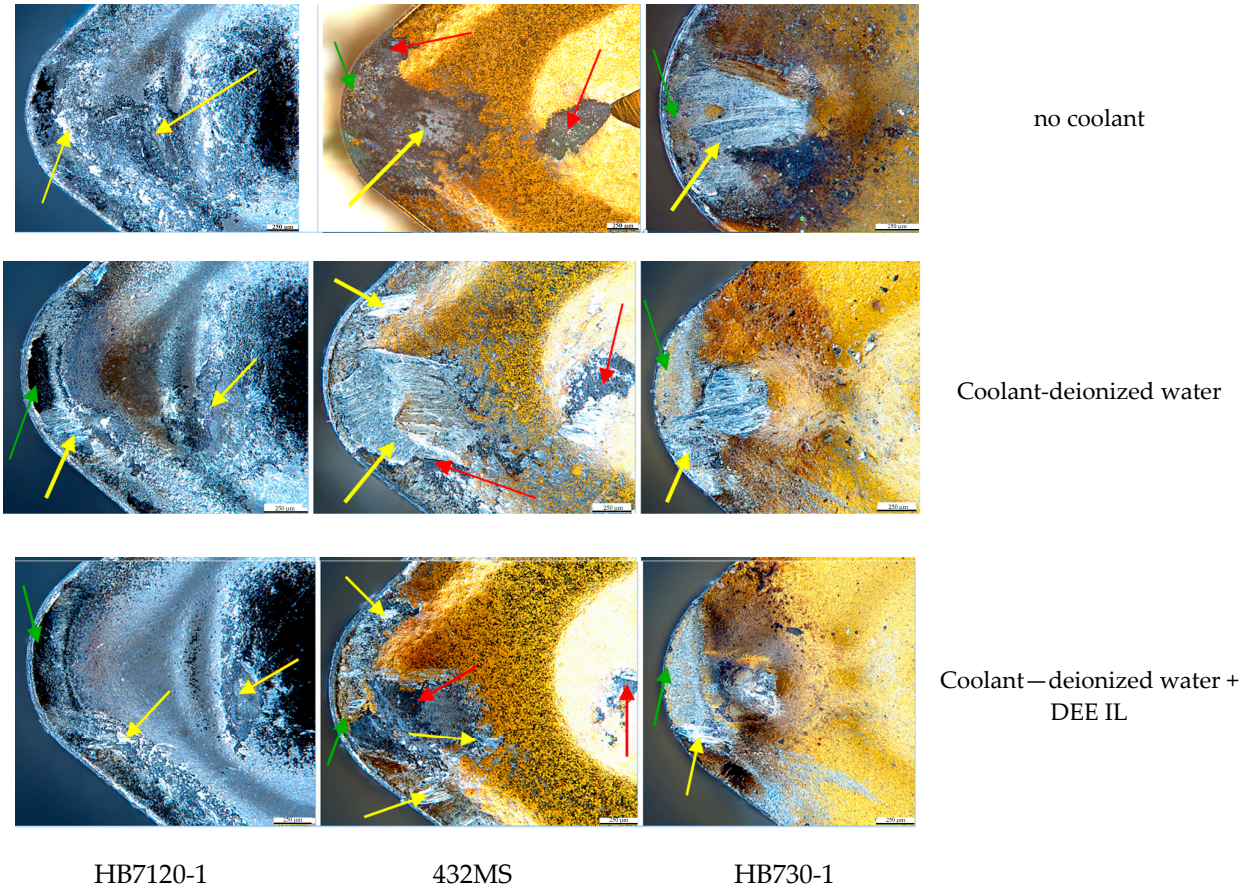
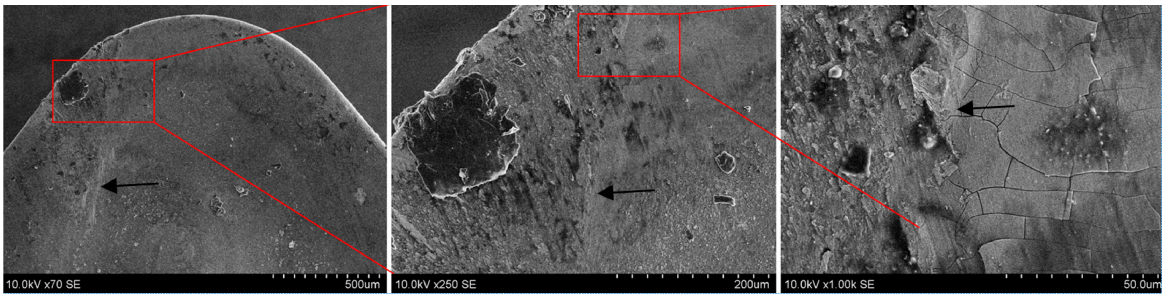


Figure 6. The view of the worn and WNMG insert rake face after T_{15} test under dry and lubricated conditions: f = 0.5 mm/rev; ap = 1 mm and V_c = 157 m/min.

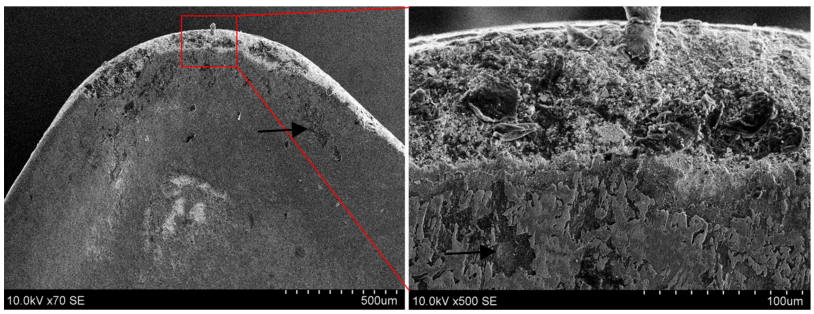
Common defects include coating system wear and the formation of a BUE, BUL, and CBBU (Figure 6). A detailed analysis of each case (dry, DW cooling, and DW + IL cooling) shows that the 432MS insert's coating system is more prone to wear (Figure 6, red arrows) than those of the HB7120-1 and HB730-1 inserts. All inserts are susceptible to BU (build-up) under dry conditions (yellow arrows), although cooling can mitigate this tendency, especially for HB7120-1. Meanwhile, significant BUE formation occurs on the 432MS insert under dry and Minimum Quantity Lubrication (MQL) conditions (QC = 1 g/min), particularly with deionized water (DW) cooling.

SEM images of the rake face after etching the alloy steel BUE from the insert surface show a more detailed view (Figures 7–9). The chip-flow line is clearly visible on the rake face of the HB7120-1 insert, with a wear zone to its right (Figure 7, black arrows). At higher magnification, the coating on the rake face in the chip-sliding zone is polished and cracked (Figure 7c, to the right of the black arrow). On the right, the undamaged surface is visible. No significant rake-edge damage or coating wear (delamination) is observed after 15 operating cycles.



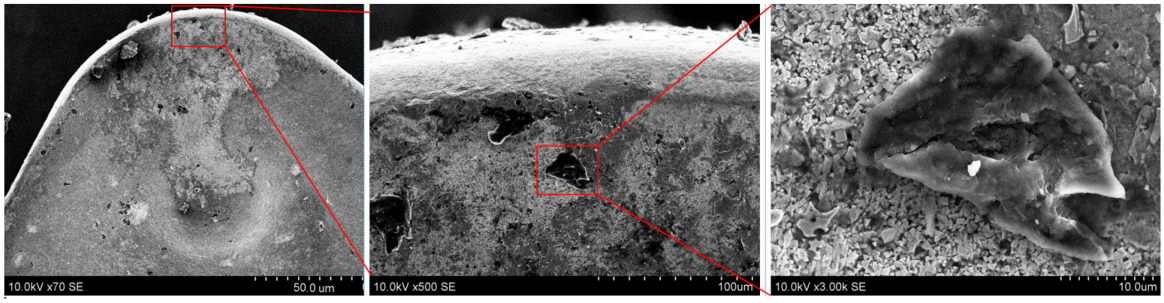
(**a**) (**b**) (**c**)

Figure 7. The SEM view of the insert rake face, worn and etched in iron chloride ($FeCl_3$) WNMG HB7120-1 insert rake face after the T_{15} test under dry conditions. (**a**) Overall view of the insert tip; (**b**,**c**) enlarged views of the selected segment: f = 0.5 mm/rev; ap = 1 mm and V_c = 157 m/min. Note: A crystal-like foreign body is a piece of debris.



(**a**) (**b**)

Figure 8. The SEM of the wear-tested and etched in iron chloride ($FeCl_3$) WNMG 432MS insert rake face after T_{15} dry conditions. (**a**) overall view of the insert tip; (**b**) enlarged view of the selected segment: f = 0.5 mm/rev; ap = 1 mm and V_c = 157 m/min.



(**a**) (**b**) (**c**)

Figure 9. The SEM of the wear-tested and etched in iron chloride ($FeCl_3$)WNMG HB730-1 insert rake face after the T_{15} test under dry conditions. (**a**) general view of the insert tip; (**b**,**c**) enlarged view of the selected segments: f = 0.5 mm/rev; ap = 1 mm and V_c = 157 m/min.

Figure 8 presents the SEM view of insert 432MS. In this case, the damage to the insert's cutting edge and surface is more severe. Micro-wear of the cutting edge and the micro-delamination of the coating-system layers are clearly visible in the SEM image (Figure 8, black arrows).

The most significant surface damage was observed on insert HB730-1. This included wear on the rake edge (a smoothed edge surface, Figure 9b) and coating wear (a light, mushroom-shaped spot, Figure 9a). At higher magnification, the grain structure (Figure 9c, left) of the powder composite insert and a remaining coating patch are visible (Figure 9c, right).

In summary, it can be clearly seen that if the chip breaker is as close to the rake edge as in the HB730-1 insert (approximately 700 µm, Figure 3c), the chip is in stronger contact with the cutting edge and the chip breaker from the beginning of cutting (Figures 4 and 5). Traces of adhesion of the AISI 316L steel to the insert are visible on the entire rake surface up to the ball segment of the chip breaker (Figure 9a). Analysis of images of the insert after the longer T_{15} test shows that the BUE at the chip breaker increases sharply with increasing ap and decreasing V_c. After a certain time, the gap between the cutting edge and the chip breaker is covered with a build-up layer (BUL) of metal to be cut due to adhesion processes, and the chip slides on this BUL layer (Figures 4 and 6). In other cases, when the chip breaker is farther away (approximately 1350 µm for HB7120-1 and 2600 µm for 432MS), BUE or BUL growth intensity may also be linked to differences in rake-face roughness and other insert characteristics. Figure 10 shows the cutting-force measurement results.

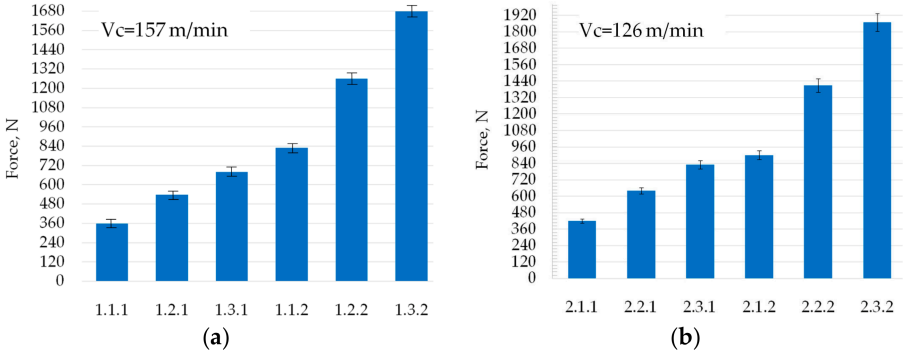


Figure 10. Dependence of cutting force on the cutting parameters *ap* and *f* (x axis as defined in Table 1) as wel as (**a**) cutting speed V_c = 157 m/min and (**b**) cutting speed V_c = 126 m/min.

It was observed that the cutting force F_c increased significantly as the cutting speed V_c decreased and the feed f and depth of cut ap increased, as expected.

A more in-depth analysis of the machined-surface roughness was not among the primary objectives of this experiment at this stage, although preliminary roughness measurements were performed. Considering the R_z value alone, no specific case shows clearly distinct characteristics. However, certain differences in surface profiles are observable. Figure 11 presents the surface profiles of one insert processed under different conditions.

After cycle T1, the machined surface profile has a "thread" shape in all cases (Figure 11a). As the number of cycles increases, the built-up edge (BUE) grows and influences the machined surface topography. When turning with the HB730-1 insert—whether dry or with standard cooling—the profiles show more tearing (Figure 11b), while cooling with the DW + IL suspension produces a more regular profile. However, the latter profile displays a characteristic notch at the edge of the insert tip (Figure 11c).

The results encourage continued experimentation to evaluate how cutting-insert parameters influence BUE formation and, in particular, machined-surface topography—specifically parameters such as R_q, R_{sk}, and R_{ku}, which may influence the surface's tribological properties in the future.

The next section explains in more detail the relationship between insert characteristics and the formation and growth of the BUE.

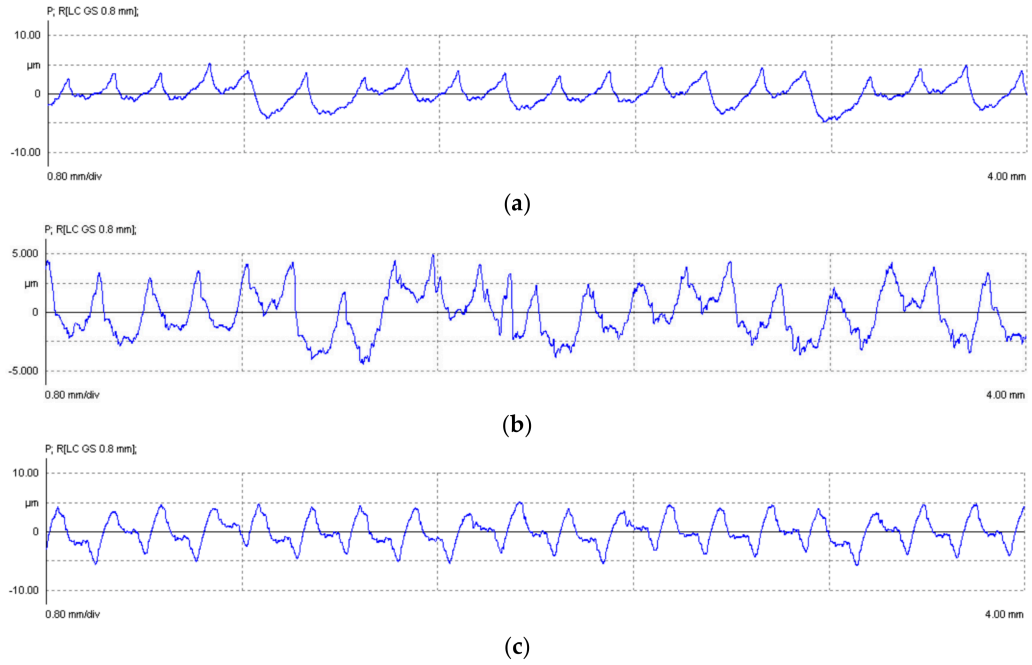


Figure 11. Profiles of AISI 316L steel surfaces machined with the HB730-1 insert: (**a**) after T_1 under dry conditions; (**b**) after T_{15} with DW cooling; (**c**) after T_{15} with DW + IL cooling. f = 0.2 mm/rev; ap = 1 mm.

4. Discussion

The profile roughness parameters offer complementary insight into the rake-face texture of the inserts examined. R_q reflects the magnitude of the profile-height deviations, while R_{sk} and R_{ku} describe the form of the profile-height distribution. Positive R_{sk} values indicate a distribution skewed toward surface peaks, whereas negative values indicate a skew toward valleys. R_{ku} represents the kurtosis of the height distribution: values close to 3 suggest an approximately Gaussian distribution, values greater than 3 imply more pronounced extreme height features, and values less than 3 indicate a flatter distribution.

Of the measured profiles, 432MS showed the highest R_a and R_q values (1.242 and 1.564 µm, respectively), while HB730-1 had the smallest values (0.938 and 1.163 µm, respectively). All three inserts had positive R_{sk} values, ranging from 0.047 for HB7120-1 to 0.162 for HB730-1. R_{ku} ranged from 2.687 for HB730-1 to 3.644 for 432MS. Overall, these results indicate variations in the rake-face profiles chosen across the three inserts.

Friction force for dry contact can be expressed as $F_d = \alpha.A_r\tau_d$, where F_d is the dry contact frictional force, α. is the fraction of dry contact area at the interface, τ_d is the average shear strength of dry contact at the interface, and A_r is the real area of contact [24]. The actual contact conditions at the tool–chip interface can be influenced by both the size and spatial distribution of surface-height features. Here, R_a and R_q describe the amplitude of the profile-height fluctuations, while R_{sk} and R_{ku} add information about the form of the height distribution. These parameters could therefore affect friction and adhesion; however, their separate contributions cannot be determined in the present work because the inserts also vary in coating composition and chip-breaker geometry.

In this study, the observed link between the initial roughness of the rake face and BUE formation is qualitative. The area, height, and volume of the BUE were not measured quantitatively; as a result, the current data set does not allow a statistical correlation between BUE size and individual roughness parameters.

In this study, surface roughness was not varied independently because the commercial inserts examined also varied in coating composition and chip-breaker geometry. As a

result, the effects of specific roughness parameters cannot be fully isolated from other insert features.

In addition, we determined the profile roughness parameters from a single selected profile for each insert. As a result, we could not statistically assess the repeatability or spatial variability of the measurement within an insert, and the reported roughness values should be regarded as descriptive features of the profiles analyzed. Table 3 presents the summarized results.

Table 3. Summary table of key quantitative and qualitative results.

Parameter	HB7120-1	432MS	HB730-1		Notes
R_a, µm	0.995	1.242	0.938		
R_q, µm	1.257	1.564	1.163		
R_{sk}	0.047	0.140	0.162		
R_{ku}	2.806	3.644	2.687		
Cutting-edge–chip breaker distance, µm	~1350	~2600	~700		
V_c = 126 m/min	High	High	High	Dry	Sensitivity to BUE
	Low	High	Moderate	DW	
	Low	High	Moderate	DW + IL	
V_c = 157 m/min	Low	Moderate	High	Dry	
	Low	Moderate	High	DW	
	Low	Low	Moderate	DW + IL	
V_c = 157 or 126 m/min	Moderate	Moderate	High	Dry	Sensitivity to CBBU
	Moderate	Moderate	Moderate	DW	
	Low	Low	Low	DW + IL	
V_c = 157 or 126 m/min	Moderate	High	High	Dry	Sensitivity to SBU
	Low	High	Moderate	DW	
	Low	Moderate	Low	DW + IL	
V_c = 157 m/min	Low	High	Moderate	Dry	Sensitivity to wear
	Low	High	Moderate	DW	
	Low	Moderate	Low	DW + IL	

Machining AISI 316L steel is complicated because of its tendency to strain harden [25], its high ductility [9,10], and the high stresses in the contact zone [26]. In addition, corrosion-resistant austenitic steels have a high coefficient of friction and a high coefficient of thermal expansion in the cutting zone, along with low thermal conductivity. These factors increase heat generation in the cutting zone, as shear and friction energy are directly proportional to shear rate and cutting speed [27]. As a result, the material properties change due to the interaction of the contacting surfaces. The most important types of tool wear include wear craters, flank wear, notch wear, and BUE (SBU). These phenomena were clearly observed in the present study. Traditionally, cutting speed directly affects temperature rise, even when a cryogenic medium is used [23]. As temperature increases, the material's shear strength decreases and its plasticity increases; chip separation from the workpiece becomes more difficult, and surface roughness increases [27]. In our case, the results were slightly different. If only the roughness R_z (R_a) is considered, the inserts produced smoother surfaces in the presence of a BUE (SBU), consistent with reports that BUE formation can sometimes positively affect workpiece surface roughness because BUE formation increases the tool nose radius [28]. Based on this information, the study presents the results obtained.

The WNMG 080408 HB730-1 insert used in the experiment differed from the others because it had a spherical chip breaker (CB) close to the rake edge (Figure 3c). Analysis of the images in Figures 4 and 5 shows that at V_c = 157 m/min, the contact between the chip

and the rake surface and the CB is relatively small. At higher cutting speeds and smaller depths of cut, F_c is lower, and the chip is pressed less against the insert. Comparison of the new insert in Figure 3 with the insert after the T_1 test in Figure 4 shows that a BUE forms on the insert edge and on the rake face or chip breaker right at the beginning of cutting. It appears that the chip does not slide all the way over the insert surface to the CB. After the BUE and SBU material was etched away, signs of wear were already visible on the CB and the insert edge. A wear trace produced by the chip edge is visible on the rake surface (Figure 4, CEL), the same as in Figures 5 and 6.

As the cutting depth increases, the chip becomes thicker, forces increase, and diffusion and adhesion phenomena intensify. For this reason, the contact zone extends from the cutting edge along the rake face toward the CB (Figures 4 or 6). The CBBU grows toward the cutting edge, and during the longer cutting process, it fuses with the BUE into the SBU. The chip does not slide on the insert surface, but on the continuous build-up layer that has formed. As the cutting speed decreases, F_c increases, the chip is pressed more strongly against the insert on the rake face, and the sliding speed decreases. The SBU forms faster because these conditions appear to favor CBBU growth.

After the formation of an SBU from AISI 316L steel, the chip slides with greater resistance due to the inherently sticky nature of AISI 300-series steels, as described by Wagha et al. [29].

As a rule, the BUE can be stable or unstable and is regularly "carried away" by chips [30]. However, in the investigated case, the BUE is more stable and lasts longer on the HB7120-1 insert. This may be explained by the greater irregularity of the machined surface (profilograms in Figure 11). The SBU supports the BUE to some extent and prevents the chip from "taking" the BUE with it. In this way, the BUE forms a "new" cutting edge and is involved in SBU formation. At lower cutting speeds, this phenomenon strongly affects roughness parameters and machined surface quality when turning AISI 316L steel, especially when turning dry. Future studies should evaluate the minimum effective coolant flow rate based on the type of insert chip breaker and the texture of the rake face.

5. Conclusions

The tests were performed by turning the outer surface of an AISI 316L steel bar using cutting conditions selected according to the manufacturer's recommendations for the WNMG 080408 inserts (HB7120-1, HB730-1, and 432MS) and the available settings of the manually controlled lathe. Cutting was performed under dry conditions and with minimum-quantity lubrication using deionized water (DW) or a DW-based ionic-liquid (IL) suspension.

As the cutting speed V_c decreased, the cutting forces F_c increased. The increase in F_c was directly proportional to the increase in feed f and the depth of cut *ap*.

The examined inserts differed in rake-face geometry and in profile roughness features. Of the measured profiles, 432MS had the highest R_a and R_q values, while HB730-1 had the lowest R_a and R_q values and the highest R_{sk} value. The estimated cutting edge-to-chip-breaker distances were approximately 1350 µm for HB7120-1, 2600 µm for 432MS and 700 µm for HB730-1. The variations in BUE formation relate to the combined properties of the inserts studied, rather than to surface roughness alone.

The dynamics of the continuous built-up layer (SBU) on the HB730-1 insert, whose chip breaker is located close to the rake edge, were clarified during dry turning under conditions of decreasing cutting speed. As the chip slides along the rake face, the SBU grows intensively from the cutting edge toward the chip breaker (CB) because the "stickiness" of AISI 316L promotes diffusion and adhesion at the insert surface. When the chip reaches the CB, the BUE on the chip breaker (CBBU) also grows toward the cutting edge because

the CB restricts chip sliding. In the absence of cooling and lubrication, the BUE and CBBU eventually merge to form a continuous SBU. This SBU supports the BUE and increases its stability.

A minimal cooling regime (1 g/min) using DW and an IL suspension was sufficient to reduce chip adhesion to the cutting tool and eliminate the formation of a BUE, SBU, or CBBU at cutting speeds of V_c = 157 m/min and V_c = 126 m/min.

Author Contributions: Conceptualization, S.B. and A.Ž.; methodology, A.Ž.; software, A.A. and O.K.; validation, S.B., A.Ž. and E.D.; formal analysis, A.Ž. and S.B.; investigation, A.Ž., S.T., O.K., A.A. and R.K.; resources, S.B. and E.D.; data curation, A.Ž. and S.B.; writing—original draft preparation, A.Ž. and S.B.; writing—review and editing, S.B., E.D. and R.K.; visualization, A.Ž. and A.A.; supervision, S.B. and E.D. All authors have read and agreed to the published version of the manuscript.

Funding: This research received no external funding.

Institutional Review Board Statement: Not applicable.

Informed Consent Statement: Not applicable.

Data Availability Statement: The original contributions presented in this study are included in the article. Further inquiries can be directed to the corresponding author.

Acknowledgments: During the preparation of this manuscript, the authors used Grammarly for Microsoft Word (version v1.2.289.1946; Grammarly, Inc., San Francisco, CA, USA, https://www.grammarly.com/) for the purposes of language editing and proofreading (translation, grammar, structure, spelling, punctuation, and formatting), as they are non-native English speakers. The authors declare that AI was not used in the preparation and development of the presented research, paragraphs, results, or the manuscript. The authors have reviewed and edited the output and take full responsibility for the content of this publication.

Conflicts of Interest: The authors declare no conflicts of interest.

Abbreviations

The following abbreviations are used in this manuscript:

BUE	Built-Up Edge
SBU	Surface Build-Up
CBBU	Chip-Breaker Build-Up
CEL	Chip-Edge Line
CZ	Chip-Sliding Zone
DW	Deionized Water
ILs	Ionic-Liquid Suspension

References

1. Precedence Research. Available online: https://www.precedenceresearch.com/stainless-steel-market (accessed on 19 June 2026).
2. Market.us. Available online: https://market.us/report/stainless-steel-market/ (accessed on 19 June 2026).
3. Kaladhar, M.; Subbaiah, K.V.; Rao, C.S. Machining of austenitic stainless steels—A review. *Int. J. Mach. Mach. Mater.* **2012**, *12*, 178–192. [CrossRef]
4. Kumar, A.; Sharma, R.; Kumar, S.; Verma, P. A review on machining performance of AISI 304 steel. *Mater. Today Proc.* **2022**, *56*, 2945–2951. [CrossRef]
5. Ishfaq, K.; Anjum, I.; Pruncu, C.I.; Amjad, M.; Kumar, M.S.; Maqsood, M.A. Progressing towards sustainable machining of steels: A detailed review. *Materials* **2021**, *14*, 5162. [CrossRef] [PubMed]
6. Leksycki, K.; Feldshtein, E.; Ociepa, M. On the effect of the side flow of 316L stainless steel in the finish turning process under dry conditions. *Facta Univ. Ser. Mech. Eng.* **2021**, *19*, 335–343. [CrossRef]
7. Nur, R.; Noordin, M.Y.; Izman, S.; Kurniawan, D. Machining parameters effect in dry turning of AISI 316L stainless steel using coated carbide tools. *Proc. Inst. Mech. Eng. Part E J. Process. Mech. Eng.* **2017**, *231*, 676–683. [CrossRef]

8. Baharum, Z.; Affandi, M.N.T.; Yacob, A.; Ali, R. The critical factors for built up edge formation in stainless steel milling. *Int. J. Adv. Trends Comput. Sci. Eng.* **2020**, *9*, 282–288. [CrossRef]
9. Aby, M.P.; Chakraborty, K. Some studies on the machining behaviour of 316L austenitic stainless steel. *Mater. Today Proc.* **2022**, *56*, 681–685. [CrossRef]
10. Liao, Z.; Monaca, A.; Murray, J.; Speidel, A.; Ushmaev, D.; Clare, A.; Axinte, D.; M'Saoubi, R. Surface integrity in metal machining—Part I: Fundamentals of surface characteristics and formation mechanisms. *Int. J. Mach. Tools Manuf.* **2021**, *162*, 103687. [CrossRef]
11. Ahmed, Y.S.; Rabinovich, G.F.; Paiva, J.M.; Wagg, T.; Veldhuis, S.C. Effect of built-up edge formation during stable state of wear in AISI 304 stainless steel on machining performance and surface integrity of the machined part. *Materials* **2017**, *10*, 1230. [CrossRef] [PubMed]
12. Equbal, A.; Equbal Md, E.; Equbal Md, I.; Ravindrannair, P.; Khan, Z.A.; Badruddin, I.A.; Kamangar, S.; Tirth VJaved, S.; Kittur, M.I. Evaluating CNC milling performance for machining AISI 316 stainless steel with carbide cutting tool insert. *Materials* **2022**, *15*, 8051. [CrossRef] [PubMed]
13. Ribeiro, F.S.F.; Lopes, J.C.; Bianchi, E.C.; Sanchez, L.E.d.A. Applications of texturization techniques on cutting tools surfaces—A survey. *Int. J. Adv. Manuf. Technol.* **2020**, *109*, 1117–1135. [CrossRef]
14. Šramhauser, K.; Kraus, P.; Špalek, F.; Černý, P.; Ufitikirezi, J.d.D.M.; Zoubek, T.; Strob, M.; Kononets, Y.; Kříž, P.; Vochozka, V. Intercomparison of indexable cutting inserts' wear progress and chip formation during machining hardened steel AISI 4337 and austenitic stainless steel AISI 316 L. *Materials* **2024**, *17*, 5418. [CrossRef] [PubMed]
15. Zeilmann, R.P.; Delgado, L.A.P.; Subtil, J.L.N.S. Effect of cutting edge preparation by drag finishing on the tool wear in milling of steel. *Int. J. Adv. Manuf. Technol.* **2026**, *143*, 2581–2596. [CrossRef]
16. Barari, N.; Niknam, S.A.; Mehmanparast, H. Tool Wear Morphology and Life under Various Lubrication Modes in Turning Stainless Steel 316L. *Trans. Can. Soc. Mech. Eng.* **2020**, *44*, 352–361. [CrossRef]
17. Saketi, S.; Bexell, U.; Olsson, M. Wear Mechanism of Cemented Carbide Cutting Tool in the Turning of 316L Stainless Steel. In Proceedings of the 18th Nordic Symposium on Tribology—NORDTRIB, Uppsala University, Uppsala, Sweden, 18–21 June 2018.
18. Mallick, R.; Kumar, R.; Panda, A.; Sahoo, A.K.; Das, D. Synthesis of an ionic liquid-based cutting lubricant and its performance comparison with mineral oil in hard turning. *Lubricants* **2025**, *13*, 166. [CrossRef]
19. Davis, B.; Schueller, J.K.; Huang, Y. Study of ionic liquid as effective additive for minimum quantity lubrication during titanium machining. *Manuf. Lett.* **2015**, *5*, 1–6. [CrossRef]
20. Saketi, S.; Bexell, U.; Östby, J.; Olsson, M. On the diffusion wear of cemented carbides in the turning of AISI 316L stainless steel. *Wear* **2019**, *430–431*, 202–213. [CrossRef]
21. Gerth, J.; Gustavsson, F.; Collin, M.; Andersson, G.; Nordh, L.-G.; Heinrich, J.; Wiklund, U. Adhesion phenomena in the secondary shear zone in turning of austenitic stainless steel and carbon steel. *J. Mater. Process. Technol.* **2014**, *214*, 1467–1481. [CrossRef]
22. Kónya, G.; Csorba, B.; Szabó, N.; Kovács, Z.F. The effects of cutting parameters on cutting force and tribological properties of machined surface under dry turning ofAISI304L austenitic stainless steel. *J. Manuf. Mater. Process.* **2024**, *8*, 257. [CrossRef]
23. Ba, T.; Cheikh, E.; Martins, P.S.; Dumont, M.R. Statistical study of surface texture and chip formation during turning of AISI 1020 steel: Emphasis on parameters R_{sk}, R_{ku}, and R_k family and on the chip thickness ratio. *Int. J. Adv. Manuf. Technol.* **2022**, *121*, 8257–8283. [CrossRef]
24. Orra, K.; Choudhury, S.K. Tribological aspects of various geometrically shaped micro-textures on cutting insert to improve tool life in hard turning process. *J. Manuf. Proc.* **2018**, *31*, 502–513. [CrossRef]
25. Yan, X.; Hu, J.; Zhang, X.; Xu, W. Obtaining superior low-temperature wear resistance in Q&P-processed medium Mn steel with a low initial hardness. *Trib. Internat.* **2022**, *175*, 107803. [CrossRef]
26. Lu, M.; Wang, X.; Lin, J.; Chen, Y.; Du, Y. Modeling and analysis of specific cutting energy for Ti6Al4V alloy using quasi-intermittent vibration-assisted swing cutting. *Precis. Eng.* **2026**, *97*, 817–827. [CrossRef]
27. Szczotkarz, N.; Mrugalski, R.; Maruda, R.W.; Królczyk, G.M.; Legutko, S.; Leksycki, K.; Dębowski, D.; Pruncu, C.I. Cutting tool wear in turning 316L stainless steel in the conditions of minimized lubrication. *Tribol. Int.* **2021**, *156*, 106813. [CrossRef]
28. Gökkaya, H. The Effects of Machining Parameters on Cutting Forces, Surface Roughness, Built-Up Edge (BUE) and Built-Up Layer (BUL) During Machining AA2014 (T4) Alloy. *Stroj. Vestn. J. Mech. Eng.* **2010**, *569*, 584–593.
29. Wagha, S.S.; Kulkarnib, A.P.; Sargade, V.G. Machinability studies of austenitic stainless steel (AISI 304) using PVD cathodic arc evaporation (CAE) system deposited AlCrN/TiAlN coated carbide inserts. *Procedia Eng.* **2013**, *64*, 907–914. [CrossRef]
30. Yaman, K.; Tekiner, Z. Investigation of the effect of built-up edge on chip morphology at the cutting edge during turning operation. *J. Polytech.* **2024**, *27*, 2325–2333. [CrossRef]

Disclaimer/Publisher's Note: The statements, opinions and data contained in all publications are solely those of the individual author(s) and contributor(s) and not of MDPI and/or the editor(s). MDPI and/or the editor(s) disclaim responsibility for any injury to people or property resulting from any ideas, methods, instructions or products referred to in the content.